Discrete elastic model for two-dimensional melting

Yves Lansac,[1] Matthew A. Glaser,[2] and Noel A. Clark[2]
[1]*LEMA, UMR 6157 CNRS-CEA, Université François Rabelais, 37200 Tours, France*
[2]*Condensed Matter Laboratory, Department of Physics, and Ferroelectric Liquid Crystal Materials Research Center, University of Colorado, Boulder, Colorado 80309, USA*
(Received 7 September 2005; published 3 April 2006)

We present a network model for the study of melting and liquid structure in two dimensions, the first in which the presence and energy of topological defects (dislocations and disclinations) and of geometrical defects (elemental voids) can be independently controlled. Interparticle interaction is via harmonic springs and control is achieved by Monte Carlo moves which springs can either be orientationally "flipped" between particles to generate topological defects, or can be "popped" in force-free shape, to generate geometrical defects. With the geometrical defects suppressed the transition to the liquid phase occurs via disclination unbinding, as described by the Kosterlitz-Thouless-Halperin-Nelson-Young model and found in soft potential two-dimensional (2D) systems, such as the dipole-dipole potential [H. H. von Grünberg *et al.*, Phys. Rev. Lett. **93**, 255703 (2004)]. By contrast, with topological defects suppressed, a disordering transition, the Glaser-Clark condensation of geometrical defects [M. A. Glaser and N. A. Clark, Adv. Chem. Phys. **83**, 543 (1993); M. A. Glaser *et al.*, *Springer Proceedings in Physics: Dynamics and Patterns in Complex Fluids* (Springer-Verlag, Berlin, 1990), Vol. 52, p. 141], produces a state that accurately characterizes the local liquid structure and first-order melting observed in hard-potential 2D systems, such as hard disk and the Weeks-Chandler-Andersen (WCA) potentials (M. A. Glaser and co-workers, see above). Thus both the geometrical and topological defect systems play a role in melting. The present work introduces a system in which the relative roles of topological and geometrical defects and their interactions can be explored. We perform Monte Carlo simulations of this model in the isobaric-isothermal ensemble, and present the phase diagram as well as various thermodynamic, statistical, and structural quantities as a function of the relative populations of geometrical and topological defects. The model exhibits a rich phase behavior including hexagonal and square crystals, expanded crystal, dodecagonal quasicrystal, and isotropic liquid phases. In this system the geometrical defects effectively control the melting, reducing the solid-liquid transition temperature by a factor of ~ 3 relative to the topological-only case. The local structure of the dense liquid has been investigated and the results are compared to that from simulations of WCA systems.

DOI: 10.1103/PhysRevE.73.041501 PACS number(s): 61.20.Ja, 64.60.−i, 61.20.Ne

I. INTRODUCTION

In the 1960's Bernal tried to understand the liquid phase near freezing by characterizing its local organization as arrangements of atoms (modeled by hard spheres) into various kinds of polygons [1–4]. These geometrical defect structures were defined by the bonds to the centers of neighboring particles and formed the holes responsible for the lower density of the liquid relative to the close packing of the solid. In the modern statistical physics of liquids Bernal's primarily descriptive approach has been largely abandoned in favor of the use of integral equations [5], which enable calculation of pair correlation functions and the thermodynamic properties of dense liquids. However, such methods provide little understanding of the extended multiparticle correlations characteristic of local liquid structure that so fascinated Bernal, and do not provide a mechanistic picture of the melting transition. More recently, the Bernal approach was resurrected by Glaser and Clark [6,7] who, by introducing and developing a realistic picture of geometrical defect interactions and collective behavior, described and obtained the geometrical defects in dense two-dimensional (2D) liquids in the context of a simple mechanistic model of melting. In this model the defect collectivity, driven by the reduction of local packing strain due to organization of particles into tilinglike arrangements, yielded both a first order melting transition as well as an excellent description of local structure in the liquid.

In addition to providing a useful system for developing an understanding of the local geometry of liquid structure, the two-dimensional case is even more interesting due to the role of topological defects (dislocations and disclinations) in the melting transition. In 2D the energy and entropy of dislocations and disclinations have a similar functional dependence on defect density, leading to the Kosterlitz-Thouless-Halperin-Nelson-Young (KTHNY) [8–12] predictions of melting via topological defect unbinding transitions. According to this model, the solid-liquid transition in two dimensions occurs via two second order phase transitions, corresponding to the successive unbinding of dislocations and disclinations. In addition, a new phase, the hexatic phase with only dislocations unbound and characterized by short-range positional order and by quasi-long-range bond orientational order, is predicted to appear between the solid and the liquid.

The KTHNY scenario has received clear experimental confirmation as the correct picture of melting in the case of a 2D system of particles interacting with a soft dipole-dipole $(1/r^3)$ repulsion [13]. Gompper and Kroll [14] have used an elastic model bearing some common features with our

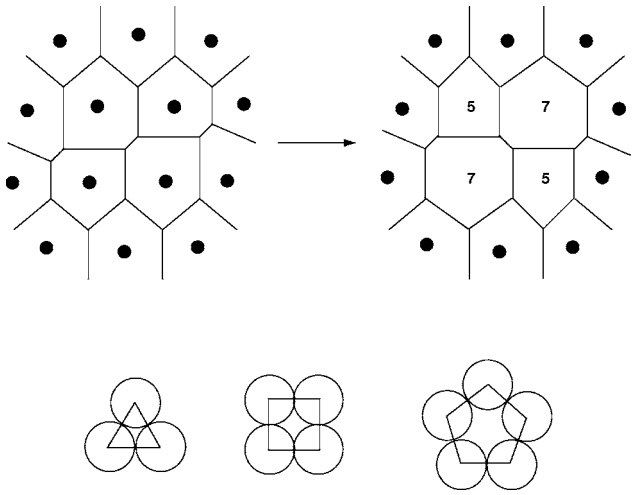

FIG. 1. Voronoi construction for two nearly square arrangements of particles, showing how a small displacement of the particles can create a disclination quadrupole (right) from a configuration with no disclination. Schematic representation of the holes created by a geometrical nontopological defect (left).

present model (as well as significant differences, especially nodes represented by hard-core particles) and have found using finite-size scaling analysis strong support in favor of a melting process following the KTHNY scenario, although with a hexatic phase stable over an extremely narrow range of densities. On the other hand, experimental and simulation studies of 2D hard-potential systems [e.g., hard disk (HD), Weeks-Chandler-Anderson (WCA), Lennard-Jones], consistently show melting to be a first order transition. Our previous HD and WCA molecular dynamics simulations [6] have focused on the mechanism of melting and were devoted to a better intuitive understanding of the microscopic structure of a dense liquid. The results have shown that the melting occurs via a first order phase transition and that an important aspect of the transition is the appearance of geometrical (nontopological) disorder in the liquid phase. This disorder manifests itself in the presence of a significant degree of square lattice coordination (holes, see Fig. 1) in the liquid phase with particles adopting local arrangements characteristic of plane tiling composed of squares and equilateral triangles (ST tiling) [15–17]. Dense random packings (DRPs) [18,19] exhibit the same kind of ST tilinglike structures and are quite supportive of the fact that geometrical constraints play an important role in melting and liquid structure of "hard" particles. Topological defects are responsible for the loss of long range positional order characteristic of a liquid, but the geometrical excitations, not captured by the Voronoi [20] or Delaunay (the dual of the Voronoi representation) representations, formed by almost local square organization of the particles may contribute significantly to the thermodynamics (i.e., the change in density) occurring at the melting transition. Both topological and geometrical defects are the fundamental excitations that control the transition and formed the basis of our mechanistic picture of a dense liquid: the two-dimensional melting is a condensation of localized, thermally generated geometrical, *and* topological defects. Condensation is a phase transition resulting from attractive interactions between the excitation or particles of interest, i.e., in our case between the defects. The scalar order parameter of the transition (i.e., the number density of geometrical defects) is unrelated to the symmetry-derived order parameters and then the global symmetry change could be very well seen as a side effect of the defect condensation mechanism that drives the 2D melting transition. This picture is similar to the one obtained in a three-dimensional liquid by the mechanistic models of Bernal. This is not too surprising, because in the framework of a melting transition driven mainly by packing constraints, global symmetry is irrelevant in determining the characteristics of the melting transition, then there is no compelling reason that 3D melting should be qualitatively different from 2D melting.

Based on these observations, we present here a discrete elastic model constituted by a network of nodes connected together by elastic springs which capture the essential features of the structure of a liquid not too far from the freezing point. This model can be seen as an analog of the mechanistic models from Bernal, modern computer, and Monte Carlo techniques allowing a much more powerful tool to probe the statistical structure of liquids. In the first part of the article, we describe the discrete elastic model and the numerical methodology applied in order to mimic a dense liquid. In the second part we present the phase diagrams obtained with the model as a function of the relative populations of the two different kind of excitations. Then the structure of the dense liquid is discussed in detail and various thermodynamics and structural quantities are computed and compared with our earlier simulations, hereafter referred as WCA liquid. In conclusion, we summarize our results and discuss their pertinence to support the melting mechanism we have proposed.

II. DISCRETE ELASTIC MODEL

From the WCA liquid study, the 2D melting can be seen as a defect condensation transition involving both geometrical and topological defects. Topological defects (disclinations) are characterized by a number of nearest neighbors different from 6 (i.e., different from what is expected for a perfect triangular lattice). A node (playing in our model the role of the center of mass of a disklike particle) having five nearest neighbors is identified as a -1 disclination due to the fact that it corresponds to the removal of a 60° wedge of material at a microscopic level, while a node having seven nearest neighbors is identified as a $+1$ disclination, corresponding to the addition of a 60° wedge of material at a microscopic level. An isolated disclination corresponds to the 60° rotation of a vector oriented along one of the lattice directions upon parallel transport around a closed circuit enclosing the disclination and is responsible for the loss of long-range bond-orientational order in the system. An isolated dislocation is formed by a bound pair of disclination of opposite strength and corresponds to a nonzero Burger vector (the amount by which a Burger's circuit fails to close around a dislocation) and is responsible for the loss of quasi-long-range positional order in the system. In the liquid phase, a Burger's circuit is an ill-defined quantity since no lattice is present.

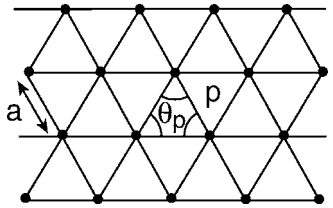

FIG. 2. Schematic representation of the discrete elastic model, in which each node is connected to its nearest neighbors with an elastic spring of equilibrium length a and elastic constant K_r. In addition, bond-angle springs with equilibrium bending angle θ_p and elastic constant K_θ are used between adjacent springs.

Geometrical defects are nontopological defects and large amplitude localized geometrical distortions in which the particles have adopted a nearly square organization but are not associated with a disclination or dislocation (see Fig. 1). There is a clear tendency for particles in the dense 2D WCA liquid to form local arrangements characteristic of ST tiling. The WCA liquid can be usefully described as polygon packing or imperfect tiling (i.e., formed with deformable tiles), and the effect of packing constraints on the local geometry of these dense systems can be embodied in particular tiling rules that condition the local arrangement of the polygons. The volume increase upon melting is directly related to the creation of polygons having more than three sides.

The discrete elastic model is built to mimic the polygon tiling representation obtained from the Delaunay representation in the WCA liquid and to reproduce the two kinds of excitations responsible for the melting transition and the dense liquid structure. It is constituted by a network of nodes (playing the role of the center of mass of the disk particles of the WCA liquid) connected by springs. In addition to the bond stretching springs, bond angle bending springs have been considered in order to avoid unphysical folding of the network at high pressure (Fig. 2). A solidlike local structure is characterized by a triangular equilateral network of springs connecting nodes, or equivalently by a plane tiling of nearly perfect equilateral triangles. One of the main interests of the model over its real-particle counterpart is that it is possible to probe almost independently the effect of topological and geometrical excitations on the melting transition and the resulting dense liquid structure.

Within the framework of the discrete elastic model, the creation of topological defects is reproduced by a local change in the connectivity of the network achieved by the flipping of a given spring bond between two nodes. The network topology is locally modified, resulting in the creation of a bound-pair of dislocations [Fig. 3(a)]. Such a neutral quadrupole arrangement does not disrupt the long-range positional order of the system, but is at the origin of the subsequent creation of topological defects by unbinding mechanism. The creation of isolated dislocations then isolated disclinations from such a quadrupole is schematically depicted in Fig. 3(a).

A bond breaking achieves the creation of a geometrical defect [Fig. 3(b)]. This procedure allows the two previously connected nodes to remain in the proximity of their former nearest neighbors without being strongly bound to them, be-

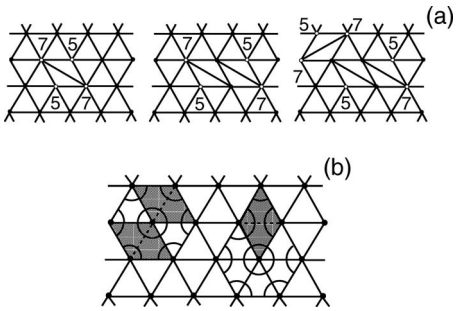

FIG. 3. Illustration of the MC moves performed on the springs (a) bond flipping to mimic the creation of topological defects (arising from the unbinding of a quadrupole); (b) bond breaking to mimic the creation of a geometrical defect.

having as nearly as second neighbors. This is a weaker effect than the change of neighborhood induced by a bond flipping. Practically, the bond breaking procedure is accompanied by an update of the equilibrium bond angles to reflect the induced change in geometry from two equilateral tiles (bond angle springs set to 60°) to one nearly-square tile (bond angle springs set to 90°) [Fig. 3(b)].

These two procedures (bond flipping and bond breaking) are suitable to mimic a system in which the populations of the two kinds of defects can be controlled and their resulting effects on the melting transition analyzed. If only bond flipping is allowed, we will talk about a topological only model, if only bond breaking is allowed, the model will be qualified of geometrical only model and if both bond flipping and bond breaking are permitted, we will talk of a topological and geometrical model. The elastic network connectivity fluctuations are responsible for the nodes diffusion in our model. Therefore two nodes initially neighbors will not necessarily remain neighbors forever, at least in the liquid phase. Finally, it is worth noticing that local, squarelike fluctuation of the triangular lattice are also present in the topological only model, and could be exhibited by using a bond dilution procedure (i.e., removal of all the bonds significantly longer than the average bond length present in the network). However, these fluctuations are, due to the constraints imposed on the model, much less favorable energetically than in the model where bond breaking is allowed. This is in this sense that a distinction has been made between the topological only model and the topological and geometrical model.

In this article we focus on the minimal model in which only triangular and square tiles (three- and four-sided polygons) and topological defects with five and seven coordination numbers are considered. This is in agreement with the extensive studies performed on the WCA liquid and the random close packing system in which it was demonstrated that these excitations are the most relevant ones.

The Hamiltonian for this system is

$$H = \frac{K_r}{2}\sum_{i,j} (\mathbf{r}_{i,j} - \mathbf{a})^2 + \frac{K_\theta}{2}\sum_{i,j,k} (\theta_{i,j,k} - \theta_p)^2 + PA, \qquad (1)$$

where the first sum is on all nonbroken bonds and the second on all the bond-angle between nonbroken bonds, $|\mathbf{a}| \equiv a$ is

the equilibrium length between the two connected nodes i and j, and θ_p is the equilibrium bond angle between nodes i, j, and k, for the polygon p considered ($\theta_p=60°$, for $p=3$, i.e., for an equilateral triangle polygon and $\theta_p=90°$, for $p=4$, i.e., for a square polygon). In the case when both topological and geometrical defects are allowed no energetic cost is associated with the flipping of a broken bond. That is related to the fact pointed above, that a quadrupole of defects is nearly topologically equivalent to no defects. K_r is the stretch elastic constant, K_θ the bend elastic constant, A the area of the system, and P the external pressure. The properties of the elastic model depend only on three dimensionless parameters, a reduced temperature t, a reduced elastic constant ratio K and a reduced pressure p defined as

$$t = \frac{k_B T}{K_r a^2}, \tag{2}$$

$$K = \frac{K_\theta}{K_r a^2}, \tag{3}$$

$$p = \frac{P}{K_r a^2}, \tag{4}$$

where k_B is the Boltzmann constant and T the temperature of the system.

The statistical mechanical properties of the discrete elastic model are investigated using Metropolis Monte Carlo (MC) [21] simulations carried out in the isobaric-isothermal ensemble. Translational node displacements are also considered in order to relax the local strain induced in the system by the creation of defects resulting in a network connectivity change. In addition, the simulation box area is allowed to fluctuate in order to insure a constant pressure in the system.

III. RESULTS

A. Phase diagrams

In order to check the ability of our model to reproduce the solid-liquid transition and in order to probe the relative importance of the two kinds of excitations in our model, we compute the (p,t) phase diagrams corresponding to the cases when geometrical only, topological only, and both geometrical and topological defects are allowed. A system with $N=100$ nodes and then $3N$ bonds is used. Additional simulations have been carried out for selected state points with larger systems ($N=400$ and $N=1024$ nodes) in order to assess finite size effects and their influence on the location of the phase boundaries. A value $K=0.1$ has been chosen for all the considered models. The effect of an increase of the elastic network stiffness will result in an increase in the liquid-solid transition temperature and its effects on the location of other phase boundaries will be studied in another work.

At each state point (p,t), a Monte Carlo sampling is used corresponding to 200 000 sweeps for equilibration and 10^6 sweeps for production. The number of MC sweeps used for equilibration has been adjusted by carefully monitoring the variations of various instantaneous thermodynamic and structural quantities (in particular the average number of topological and geometrical defects) in order to ensure a proper equilibration of the largest system-size ($N=1024$) studied. The same number of sweeps has been used on smaller-size systems. The rough location of the phase boundaries is obtained upon heating the system by successive steps Δt. Smaller steps in temperature are subsequently used in order to refine the phase boundary location. Every sweep consists in the attempting move of the N nodes, attempting move of the $3N$ bonds (i.e., only flipping in the case when topological only defects are considered, only breaking when only geometrical defects are considered and either breaking or flipping when both kinds of excitations are present) and one attempting move of the simulation box (either only the area, or only the shape or a combination of the two precedent kinds) in order to keep a pressure fluctuating around the specified value.

For each pressure, the location of the phase transition as a function of the reduced temperature, and the structure of the phases are determined by computing the equation of state, the energy, the specific heat and the magnitude of the bond-orientational order parameters. We define a m-fold local bond orientational order parameter

$$\psi_m \equiv \psi_{m_i} = \frac{1}{n_i}\sum_{j=1}^{n_i} \exp(im\theta_{ij}), \tag{5}$$

where the sum runs over the n_i nearest neighbors of particle i and θ_{ij} is the angle of the bond between particle i and its jth neighbor with respect to a reference direction. In addition we define a global m-fold order parameter

$$\Psi_m = \frac{1}{N}\sum_{i=1}^{N} \psi_m \tag{6}$$

which gives a signature of the global m-fold order present in the system. We focus here on Ψ_4, Ψ_6, and Ψ_{12} which are, respectively, sensitive to squarelike solid phase, triangular solid phase, and dodecagonal quasicrystalline (QX) phase. A liquid phase will be characterized by negligible magnitudes of these three order parameters.

The resulting phase diagrams corresponding to the geometrical only model, the topological only model, and the topological and geometrical model are presented, respectively, from top to bottom on Fig. 4. Phase boundaries are estimated by studying the variation of order parameters as a function of reduced temperature at fixed reduced pressure. An example of such behavior is shown in Fig. 5 (top) for the topological and geometrical model. The evolution of the number of topological and geometrical defects in each phase is also shown in Fig. 5 (bottom).

When only geometrical defects are allowed (Fig. 4, top) no change in symmetry is expected. The system exhibits a hexagonal crystal phase (X_h), an expanded hexagonal crystal (EX), i.e., a hexagonal crystal with a lower density due to the presence of a significant number of geometrical defects (squarelike fluctuations) and a quasicrystalline (QX) phase (dodecagonal, formed by perfect ST tiling [22–25]). A triple point (X_h, QX, EX) is located around $p \simeq 0.03$ and t

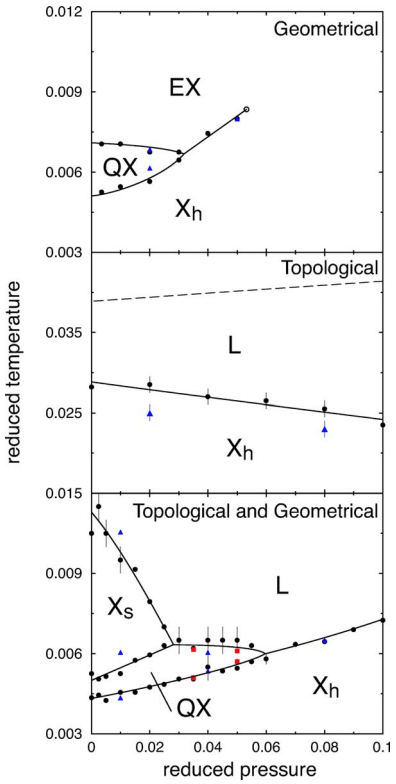

FIG. 4. (Color online) Phase diagrams obtained for a system of $N=100$ (circles) nodes with $K=0.1$ as a function of temperature t and pressure p: geometrical only defects (top); topological only defects (center), the upper dashed line being an estimate of the Kosterlitz-Thouless transition temperature; both topological and geometrical defects (bottom). X_h represents an hexagonal crystal phase, EX an expanded hexagonal crystal, X_s a square crystal phase, QX a dodecagonal quasicrystal phase, and L the dense liquid phase. Results obtained at selected pressures for $N=400$ (squares) and $N=1024$ (triangles) are also shown.

$\simeq 0.0068$. The crystal-expanded crystal transition is similar to a liquid-gas phase transition and therefore is first order and end by a critical point located around $p=0.055$. The location of this phase boundary has been characterized by the apparition of a sharp peak in the variation of the specific heat with the temperature. A representative configuration of the expanded crystal is shown in Fig. 6.

The location of the critical point has been achieved by performing additional simulations with the $N=1024$ system at a pressure $p=0.05$ and $p=0.07$. At this latter pressure no discontinuity in the order parameters or peak in the specific heat is noticeable. At pressures lower than $p=0.03$ a quasicrystalline phase is stabilized. The relative stability of the hexagonal crystal phase (i.e., a perfect tiling of the plane with equilateral triangular tiles) and the dodecagonal quasicrystalline phase (i.e., a perfect tiling of the plane with equilateral triangular and square tiles) arises as a competition between the entropy of configuration (the different arrangement of the tiles)—and to a lesser extent the entropy of vibration of the nodes—and the enthalpy (the volume change). At low enough pressure, the gain in entropy induced by a quasicrystalline phase overcomes the increase in volume for a given range of temperature ($0.005<t<0.0071$, at $p=0$),

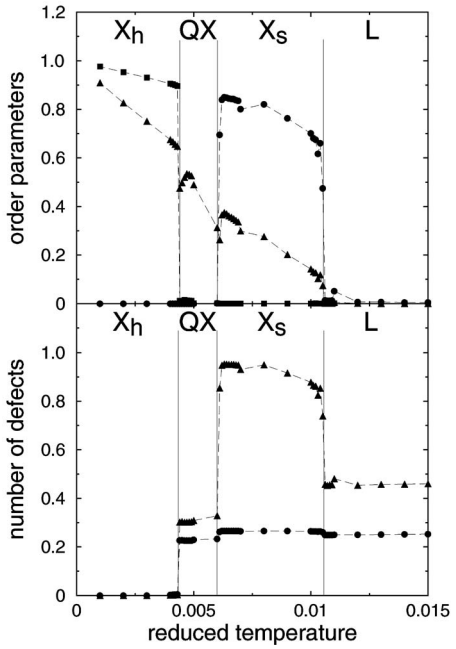

FIG. 5. Representative evolution of various order parameters (top) and defects distribution (bottom), as a function of the reduced temperature, for the topological and geometrical model, with $N=1024$ at $p=0.01$. Top: $|\Psi_4|^2$ (●); $|\Psi_6|^2$ (□); $|\Psi_{12}|^2$ (△). Bottom: topological defects (five- and seven-coordination nodes) (●); geometrical defects (broken bonds) (△). The vertical lines represent the location of X_h-QX, QX-X_s, and X_s-L phase transitions.

stabilizing the QX phase. As expected the range of stability of the QX phase with respect to the crystal phase decreases when the pressure increases. As shown for $p=0.02$, finite-size effects seem to increase the range of stability (vs the crystal phase). A representative configuration ($p=0.02$ and $t=0.0064$) of the dodecagonal quasicrystalline phase is shown in Fig. 6. The number of square polygons divided by the number of triangle polygons is ~ 0.44 and is constant within the full temperature range ($0.006<t<0.007$) of existence of the quasicrystal phase at $p=0.02$. This value is in good agreement with the value ($\sqrt{3}/4$) obtained with random tiling models (which cover the plane with a set of rigid tiles without gap) when the fraction of total tiling area occupied by square tiles is equal to the fraction occupied by triangle tiles, i.e., when the system exhibits twelvefold rotational symmetry. At the same reduced pressure, the ratio square tiles over triangle tiles is ~ 0.41 for the $N=100$ nodes system. Finite-size effects seem to decrease the probability of occurrence of geometrical defects, but do not appear to have significant role on phase boundaries.

The topological only phase diagram (Fig. 4, center) exhibits a hexagonal crystal phase (X_h) and a dense liquid due to the presence of topological defects. A phase transition between these two phases occurs over the full range of pressures studied. At each pressure, a well defined peak in the specific heat appears at the transition but due to finite-size effects it is difficult to probe the nature of the transition. The phase diagram reported here has been computed upon heating. No significant hysteresis has been observed upon cooling. Studies carried out for the larger system $N=1024$ at p

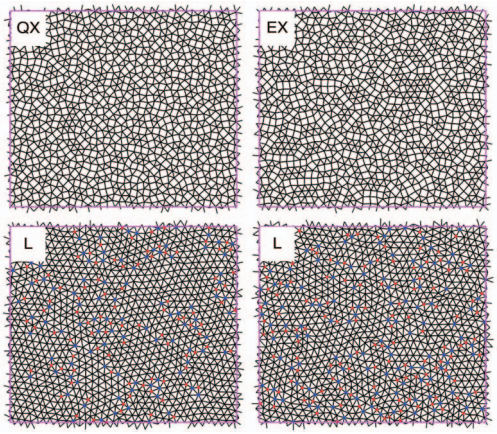

FIG. 6. (Color) Representative configurations for the geometrical only model (top) and for the topological only model (bottom), for $N=1024$. From top to bottom and from left to right: dodecagonal crystal (QX) at $p=0.02$, $t=0.0064$; expanded crystal (EX) at $p=0.02$, $t=0.008$; dense liquid (L) at $p=0.08$, $t=0.024$ ($t_c \sim 0.023$); dense liquid (L) at $p=0.08$, $t=0.028$. The red circle represent -1 topological defects and blue circles represent $+1$ topological defects. Only nonbroken bonds are represented.

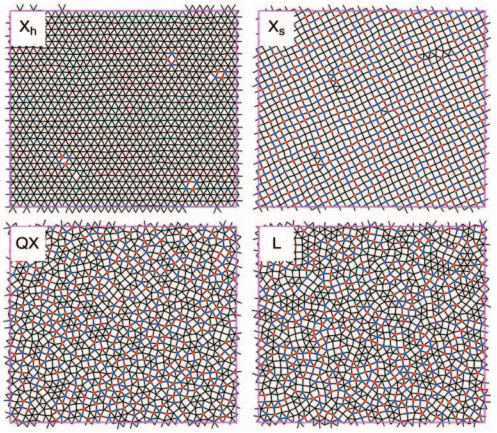

FIG. 7. (Color) Representative configurations for the topological and geometrical model for $N=1024$. From top to bottom and from left to right: hexagonal crystal (X_h) at $p=0.08$, $t=0.005$; square crystal (X_s) at $p=0.01$, $t=0.007$; dodecagonal quasicrystal (QX) at $p=0.04$, $t=0.0056$; dense liquid (L) at $p=0.08$, $t=0.007$. The red circles represent -1 topological defects and blue circles represent $+1$ topological defects. Only nonbroken bonds are represented.

$=0.02$ and $p=0.08$ indicate that the defect unbinding phase boundary is shifted downward, lowering the transition temperature by about 15%. This finite-size effect shift is comparable to that found by Grünberg *et al.* [13] as well as other 2D simulations and experiments [26–29]. Typical examples of the liquid phase are presented in Fig. 6, for a temperature close to the melting point and for a temperature deeper into the liquid phase. It is interesting to notice, from the "slope" of the solid-liquid phase transition line, using the Clapeyron relation, that our model leads to the formation of a liquid denser than its solid phase. Even if this feature is not uncommon for real liquids, it seems that in our case, this effect is related to the intrinsic nature of the discrete model. Topological defects seem to create local compressible regions, increasing the density in the system. On the phase diagram is also reported the predicted theoretical phase transition (see the Appendix) from the Kosterlitz-Thouless (KT) model that corresponds to the unbinding of pairs of dislocations. It is thought to be the upper limit for the transition to occur if no other mechanism preempts it. We notice that the KT prediction for our model is around two times larger than the transition temperatures obtained from the elastic model simulation. However, our estimations have been done at $T=0$ and taking into account the topological defects will decrease sensitively the predicted values.

The model when both topological and geometrical defects are allowed (Fig. 4, bottom) exhibits a richer phase behavior than the geometrical only model with the presence of a hexagonal crystal (X_h) phase, a square crystal (X_s) phase, a dodecagonal quasicrystal phase, and a liquid (L) phase. Typical examples of these phases are shown in Fig. 7. Two triple points are present, a (QX, X_s, L) located around $p \simeq 0.03$ and $t \simeq 0.0065$ and a (X_h, QX, L) triple point located around $p \simeq 0.06$ and $t \simeq 0.006$. If we make abstraction of the presence of the square crystal phase and we extend the upper phase boundary of the quasicrystalline phase toward $p=0$, we notice that the temperature range of existence of the quasicrystalline phase is comparable to the one present in the geometrical only model. However, the stability range in pressure of the quasicrystalline phase is almost twice as large as in the geometrical only model, due to the presence of topological defects that allow a larger gain both in entropy of conformation (by introducing tiling faults) and in entropy of vibration. By comparison with the geometrical only model, the number of square tiles divided by the number of triangle tiles is around ~ 0.45 in the quasicrytalline phase, at $p=0.02$ for the system with $N=100$ nodes. At $p=0.01$ and $p=0.04$, for the $N=1024$ system, the ratio square/triangle is roughly in the range $\sim 0.43-0.44$. Quite surprisingly, for pressure lower than $p \simeq 0.03$, a square crystal phase preempts, at high enough temperature, the full apparition of the quasicrystalline phase. This phase seems to become energetically favorable with respect to both the quasicrystalline phase and the liquid phase and quite interestingly is not present for the geometrical only model. It seems likely that this is due to a feature of the elastic model, in which bond entropy is contributing to the total entropy of the system. Because a broken bond is free to flip without any energy cost, the gain in bond entropy overcomes the loss in entropy of configuration and the increase in volume and stabilizes the square crystal with respect to the quasicrystal and the liquid phase at low enough pressure and high enough temperature. This is probably the same reason that leads, at the same pressure ($p=0.02$) and for the same temperature range, the quasicrystalline phase of the geometrical only model to exhibit slightly less squarelike polygons than the topological and geometrical model. For pressures larger than $p \simeq 0.06$ a transition occurs between a hexagonal crystal and a dense liquid. The change in symmetry of the system is governed by the topological defects. Studies at $p=0.08$ with the $N=1024$ nodes system seem to indicate, as in the geometrical only model, that the location of the solid-liquid phase boundary is not very sensitive to finite-size effects.

The most striking feature of the phase diagrams presented in Fig. 4 is the dramatic decrease (by a factor of 3 to 4) in the solid-liquid transition temperature upon inclusion of geometrical (as well as topological) defects. Evidently, the geometrical defects significantly stabilize the liquid phase relative to the solid phase. This is the potential energy per node $u=U/N$ which mainly sets the scale of the solid-liquid transition temperature t_c. At $p=0.08$ and $N=1024$ the difference in potential energy per node at the transition $\Delta u(t_c \simeq 0.023)$ for the topological only model is ~ 0.012 while for the topological and geometrical model, at $t_c \simeq 0.0065$ it is ~ 0.003, i.e., a factor 4 smaller in magnitude and of the same order of magnitude than the observed decrease in transition temperature. Upon melting, the appearance and proliferation of defects in the topological only model induces high strain on the elastic network. Geometrical defects present in the topological and geometrical model, by allowing the release of this high strain in the elastic network, are the main responsible (an increase in entropy coming from the bond entropy contribution present in our model could also play a secondary role) for the dramatic decrease of the melting temperature. This observation is quite supportive of the idea that the geometrical defects are the main responsible of the thermodynamic phase transition. In our picture the topological defects could be only a side consequence of the creation of the relevant excitations (geometrical) to the melting transition. Moreover, the transition temperatures are similar, at a given pressure, to those obtained in the case when geometrical only defects are allowed, enhancing the idea that the melting is mainly driven by the geometrical excitations.

The relative variation of volume upon melting $\Delta v/v_S$ with $\Delta v=v_L-v_S$, v_L, and v_S being, respectively, the volume of the liquid and solid phase is similar for the topological only model and for the topological and geometrical model. It is also of the same order of magnitude than for the WCA simulation. Due to the presence of the squarelike polygons, the topological and geometrical model leads to values $\sim 50\%$ larger than the topological only model and which are in closer agreement with the WCA simulation ($\Delta v/v_S \simeq 0.03$). The change of entropy per particle on melting Δs is also similar for both models but is significantly larger ($\sim 30-80\ \%$ as a function of pressure) than the one usually found ($\Delta s \simeq 0.4 k_B$) in other 2D simulations, in DRP and in theory.

System size dependence varies as the logarithm of the 2D melting transitions and is related to the inclusion of longer range fluctuations. While it is important to study such weak effects to test precisely theoretical predictions, such as the KTHNY scenario [13], they are not as important for the present exploratory work intended to assess the behavior of a new mechanistic model. Moreover, results obtained on a 10 times larger system, showing either no strong system size dependence (geometrical only and geometrical and topological models) or a 15% decrease (topological only) in the melting temperature comfort us that the qualitative features of the phase diagram are correctly captured by the present simulations.

B. Liquid structures

The structure of the dense liquid exhibited by the elastic model is investigated in more detail with the larger system, $N=1024$, at a reduced pressure $p=0.08$ for both the topological only model and the topological and geometrical model. This relatively high pressure have been chosen in order to avoid the complication in the comparison introduced by the presence of quasicrystalline and squarelike crystal structure. In order to study the microscopic structure of the dense liquid we chose a reduced temperature t_l such that $(t_l-t_c)/t_c \simeq C$, the C constant being the same for both the topological only model and the topological and geometrical model. In addition, we compare the dense liquid structure to the WCA liquid structure obtained at a density ρ_l. Figure 8 shows the radial pair correlation function and the bond-orientational correlation function for the topological and geometrical model at a reduced temperature $t=0.007$. The correlation functions exhibit the typical behavior of a dense liquid with short-range positional and bond-orientational order (within the finite-size effects).

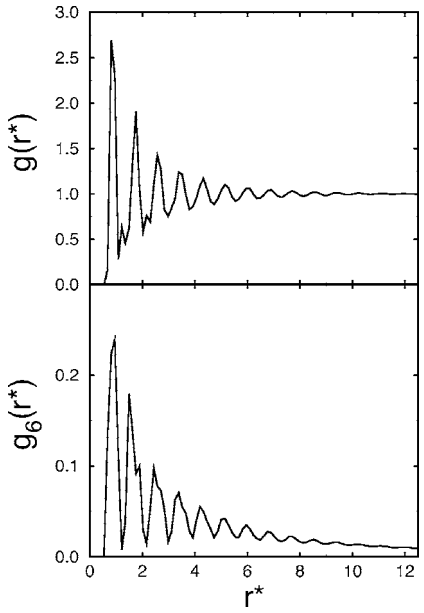

FIG. 8. Typical radial correlation function in the dense liquid phase of the topological and geometrical model, $N=1024$, $p=0.08$, $t=0.007$. Top: radial pair correlation function $g(r^*)$. Bottom: radial bond-orientational order correlation function $g_6(r^*)$ with $r^*=r/a$.

Upon the solid-liquid transition, the number of topological and geometrical defects increases dramatically. We can notice that the number of topological defects is significantly higher when bond breaking is allowed (Table I). This is mainly due to the fact that a broken bond is free to flip without energy penalty in our model. This is a feature that is present in the particle-based system for which a very slight motion of neighbor particles leads to the creation of a defect quadrupole (see Fig. 1). It could also be due to stress release or screening effects which favor the proliferation of topological defects at a lower energetic cost.

For the topological and geometrical model, the number of broken bonds (and then the number of squarelike geometrical defects) in the liquid phase is around 28%. By comparison, the WCA liquid exhibits only 15% of broken bonds at $\rho_l=0.80$ (the chosen density for our comparison), this number increasing deeper in the liquid phase (22% at $\rho_l=0.70$ [6]).

TABLE I. Probalities of occurrence of various coordination numbers.

Coordination number	Topological and geometrical	Topological only	WCA liquid
3	0	0	0
4	0	0	4.31×10^{-4}
5	0.2284	0.1020	0.1513
6	0.5432	0.7960	0.6987
7	0.2284	0.1020	0.1469
8	0	0	2.63×10^{-3}
9	0	0	2.8×10^{-8}

In Figs. 6 and 7, we notice that the topological defects are highly correlated forming chains of alternating signs. The geometrical defects are also highly correlated and aggregate in different structures. It is of interest to try to make a vertex classification in which vertices are classified according to the sequence of polygons (squares and triangles) present around a given vertex. Square-triangle (ST) tiling are models used to describe liquids [15–17] and more recently some dodecagonal quasicrystals [22–25]. There are four vertex types, hereafter referred as types A, B, C, and D, which are involved in ST plane tiling [6,7]. Our results, displayed in Table II show that vertex of types B and C are quite common in our model. In this sense, the local arrangement of three- and four-sided polygons appears to be strongly conditioned by tiling rules with a clear tendency for the three- and four-sided polygons to form structure characteristics of ST tiling. It is worth noticing that the vertex types listed in Table II account, respectively, for 99.8 and 66 % of the total vertex types present in the elastic model (topological and geometrical) and the WCA liquid. The relatively low percentage obtained for the WCA liquid is due to the fact that vertex types involving tiles with more than four sides are present (for example vertex types involving one hexagonal tile account for 22% of the total vertex types present). Our model exhibits a tendency to have more types B and C vertex than types A and B. If the population of vertex D is also low in the case of the WCA, the vertex A (corresponding to a perfect local solidlike region) are more numerous than in the elastic network model. This trend is increased further by decreasing the overall network rigidity.

TABLE II. Probalities of occurrence of various vertex types.

Vertex type	Topological and geometrical	WCA liquid
A	0.116	0.158
B	0.288	0.123
C	0.319	0.106
D	0.021	0.005
E	0.082	0.111
F	0.073	0.102
G	0.045	0.027
H	0.027	0.017
I	0.027	0.015

Of course, there are also many violations of the tiling rule. The vertex types E, F, G, H, and I correspond to tiling faults and they account respectively for 25 and 27 % of the total vertex type, respectively, for the elastic model and the WCA liquid. Vertex types E and F appear to be the most common tiling faults with type E most probable than type F for both the elastic model and the WCA liquid. From a vertex type point of view, the elastic model exhibits features that are close from those of the WCA liquid. The elastic model comes closer to the WCA liquid but the network rigidity seems still slightly too small to be able to capture one important feature of the WCA liquid, i.e., the fact that the most common vertex remains the type A, since more types B and C are present in our model.

We can see the dense liquid as a generalized tiling model in which the tiles (triangles and squares) are deformable, leading to the creation of tiling faults. A measure of the rate of deformation of a perfect ST tile can be obtained by computing the tiling charge associated to each vertex in our system. This can be done by computing [6]

$$c_\alpha = 6\left[\sum_{j=1}^{n_\alpha}\left(\frac{1}{2}-\frac{1}{p_j}\right)-1\right], \tag{7}$$

where the sum ranges over the n_α polygons which are around a vertex α, and p_j is the number of sides of the jth polygon.

It is easy to verify that the "quantum" of tiling charge is 1/10 in generalized tiling consisting of tiles having six or fewer sides, and we are expressing the tiling charge in tenths. For example vertices E and F have a tiling charge of $\pm1/2$, corresponding to ±5 tenths. Vertices corresponding to the perfect ST tiling, i.e., types A, B, C, and D, have a zero tiling charge. In our model, due to the restriction we imposed on the nature of the allowed geometrical defects, only tiling charges of strengths 0, ±5 and ±10 are possible. We notice that in our system (Table III), the larger tiling charges account only for $\sim1\%$ of the total tiling charge, suggesting that the local arrangements of polygons are strongly conditioned by tiling rules. There is a strong tendency for polygons to aggregate into structures which minimize the tiling charge around the vertices. Then, the geometrical defects have attractive, anisotropic interactions (due to their shape) that cause them to aggregate in a way that the tiling charge at a given vertex is minimized. Then the emerging picture is that the solid-liquid transition is the result of the proliferation and condensation of the geometrical defects into grain-boundary-like structure.

Extensive regions of sixfold order are present in the dense WCA liquid. The typical size of these solidlike regions increases rapidly near the freezing density. The spatial aggregation of topological defects, evident in Figs. 6 and 7 is directly related to the other prominent features of the dense liquid, i.e., the existence of the large solidlike regions that appear as rafts of nearly hexagonal Voronoi cells. This dramatic spatial inhomogeneity is a consequence of the defect condensation transition which induces the melting transition and which is seen as the qualitative key feature for a microscopic understanding of a 2D dense liquid. The same behavior has been observed in the WCA liquid.

TABLE III. Probalities of occurrence of various values of the tiling charge.

Tiling charge (in tenths)	Topological and geometrical	WCA liquid
−10	9×10^{-3}	5.67×10^{-3}
−9	0	2.25×10^{-3}
−7	0	0.0378
−6	0	3.13×10^{-4}
−5	0.1269	0.1462
−4	0	9.6×10^{-3}
−2	0	0.1056
0	0.7447	0.4017
1	0	8.26×10^{-3}
3	0	0.0901
4	0	5.7×10^{-4}
5	0.1263	0.1413
6	0	8.53×10^{-3}
8	0	0.0224
9	0	1.16×10^{-4}
10	0.0012	0.0107

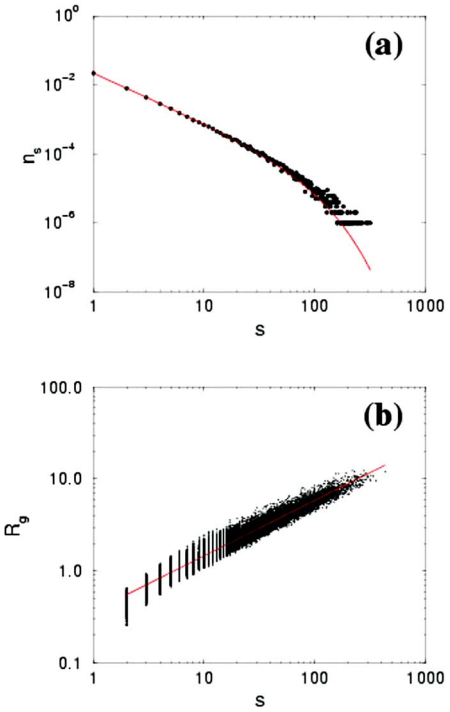

FIG. 9. (Color online) Distribution functions, in the case of the topological only model with $K=0.1$ and $t=0.025$, of (a) the cluster size n_s. The solid line represents a fit to Eq. (8); (b) the cluster radius of gyration. The solid line represents a fit to Eq. (9).

The solidlike clusters are interesting not only by themselves but also and mainly because they are a very important feature of the structure of a dense liquid and then, will play an important role on the resulting properties of the liquid, in particular on the transport properties such as viscosity. Contemporary liquid state theory is incapable of predicting the detailed characteristics of such solidlike fluctuations.

Figure 9(a) show an example, for the topological only model in the dense liquid phase, of the cluster size distribution $n_s=N_s/N$, where N_s is the average number of clusters containing s nodes and N is the total number of nodes in the system. Due to the usual normalization used in percolation theory $\Sigma_s n_s=N_c/N$, N_c being the total number of ordered clusters. The solid clusters were identified by using the criterion that the local sixfold order parameter satisfies $|\psi_6| \geqslant 0.75$. We found that the whole distributions are quite well described by the functional form

$$n_s = As^{-\tau_s}\exp(-s/\xi_s). \tag{8}$$

This is the form roughly predicted by the Fisher droplet model [30] of condensation and which represents a special case of the scaling ansatz used in percolation theory [31,32]. We have a power law behavior for small cluster size, and a crossover towards an exponential behavior for large cluster size. The fits to this functional form are quite good with, however, systematic deviation for large s. This deviation at large s is more significant in the topological and geometrical model than in the topological only model.

For the topological only model, τ_s varies in the range 1.3–1.5 decreasing with decreased temperature, while in the topological and geometrical model τ_s varies in the range 1.2–1.3 and exhibits a relatively smaller variation with a decrease in temperature. The topological only model bears more features with the WCA fluid, which exhibits values of τ_s in the range 1.2–1.5 decreasing with decreasing density. It is interesting to notice that single percolation models exhibit a constant value of τ_s for varying site or bond occupation probabilities. Though the interpretation of τ_s is not clear, it is probably connected to the geometry of the boundaries between ordered regions and then, to the tiling rules governing the dense liquid.

In the same way, for the topological only model ξ_s (which characterizes the typical size of the ordered clusters, lies in the range 20–150, decreasing with decreasing temperature while ξ_s varies in the range $\xi_s=5-10$, decreasing with decreasing temperature for the topological and geometrical model. In comparison, the WCA fluid exhibits a divergence near the freezing transition. This divergence has been attributed to finite-size effects and is connected to the presence of large-size clusters which will be of large but finite size in an infinite system but which are in the system used spanning the entire simulation box. Such an effect does not seem to happen in our case.

In conclusion, for a finite system, n_s consists of two parts: a size-independent portion at small s and a size-dependent part at large s which develops near freezing. More detailed information can be obtained by computing the shape of the clusters by calculating their radius of gyration that is related to their size s by

$$R_g = \sqrt{\frac{1}{n_s}\sum_{j=1}^{n_s} (\mathbf{r}_j - \mathbf{r}_{\text{c.m.}})^2} \propto s^{1/D_f}, \tag{9}$$

where the sum runs over the j particles at position $\mathbf{r}_j$ inside the given cluster and $\mathbf{r}_{\text{c.m.}}$ is the center of mass of the cluster. D_f is the fractal dimension of the cluster, a value of $D_f=2$ or close to 2 indicates a smooth rounded cluster while a significantly lower value indicates a rough cluster shape. To perform this analysis and due to the periodic boundary conditions the spanning clusters are identified and discarded. Figure 9(b) shows the distribution function for the radius of gyration R_g as a function of the cluster size s for the topological only model and in the dense liquid phase. A fit to the functional form gives the range of variation of D_f with the temperature. In the topological only model D_f varies in the range $D_f=1.5$ to $D_f=1.75$ near the freezing point, while in the topological and geometrical model, D_f varies in a range from $D_f=1.6$ to $D_f=1.9$ near freezing. For comparison, the WCA liquid exhibits a fractal dimension D_f varying in the range $D_f=1.6$ to $D_f=1.85$ near the freezing density. In the three cases, the same general qualitative feature is present: the solid clusters have a much smoother interface with the surrounding liquid near the freezing point than deeper inside the dense liquid phase. In addition, on a more quantitative point of view, it seems that the topological and geometrical model gives cluster shape in closer agreement with the WCA liquid than the topological only case. In particular the shape of the solid clusters is far smoother near freezing for the topological and geometrical model than for the topological only model.

IV. CONCLUSION

We have studied a simple elastic network model in order to be able to probe the relative role of the two fundamental excitations that, in our opinion, are important for the melting transition. Phase diagram obtained when only geometrical defects are present exhibits two crystal phases with hexagonal symmetry and different density as well as a dodecagonal quasicrystalline phase. When topological defects are allowed a transition between a solid and a liquid occurs. The topological and geometrical model exhibits in addition a rich phase behavior with hexagonal crystal, dodecagonal crystal, square crystal, and liquid phases. The main result is that the solid-liquid transition temperature exhibited by the model in which geometrical defects are allowed (in addition of topological defects) is decreased by a factor 3 to 4 with respect to the transition temperature exhibited in the model where geometrical defects are forbidden. Evidently, geometrical defects stabilize the liquid phase with respect to the solid phase by releasing the high strain present in the elastic network when topological only defects are present. This observation is quite supportive of the idea that if topological defects are responsible for the loss of long range positional and bond-orientational order, geometrical defects contribute significantly to the thermodynamics of the phase transition.

ACKNOWLEDGMENTS

This work was supported by NSF MRSEC Grant No. DMR 98-09555.

APPENDIX: INTERACTION PARAMETERS

The KT temperature transition is expressed by

$$k_B T = \frac{\bar{K}}{16\pi}, \tag{A1}$$

where $\bar{K}$ is the bare elastic constant and can be expressed as a function of the Lamé coefficients of the 2D solid [33]:

$$\bar{K} = \frac{4\mu B}{\mu + B}, \tag{A2}$$

where $B=-A(\partial P/\partial A)$ is the bulk modulus, and μ is the shear modulus expressed by [34]

$$\mu = -\frac{A'}{A}(1+\epsilon)^{-1}\mathcal{P}(1+\epsilon^T)^{-1}, \tag{A3}$$

where A' is the deformed volume, ϵ is the strain tensor, ϵ^T, is its transposed, and $\mathcal{P}$ is the microscopic stress tensor defined as

$$\mathcal{P}_{\alpha\beta} = \frac{1}{A'}\sum_i \sum_{j>i} r_{ij\alpha} F_{ij\beta} \tag{A4}$$

where $r_{ij\alpha}=r_{i\alpha}-r_{j\alpha}$ is the α component of the distance between particles i and j and $F_{ij\beta}$ is the β component of the force due to the particle i on particle j.

In order to have a rough analytical idea of the magnitude of the predicted KT transition we compute the Lamé coefficients in the framework of our model at $T=0$, i.e., considering that we have a perfect 2D-triangular solid lattice. Moreover we assume that the pure shear strain is infinitesimal.

At the first order in strain magnitude, the bulk and shear modulus are expressed in dimensionless variables by

$$B = \frac{\sqrt{3}}{2}\left(1 + \frac{p}{\sqrt{3}}\right), \tag{A5}$$

$$\mu = \frac{p}{2} + \frac{\sqrt{3}}{2}\left[1 + 3K\left(1 + \frac{p}{\sqrt{3}}\right)\right]. \tag{A6}$$

Then, the dimensionless KT transition temperature $t_{\text{KT}} = k_B T_{\text{KT}}/K_r a^2$ is

$$t_{\text{KT}} = \frac{p + \sqrt{3}\left[1 + 3K\left(1 + \frac{p}{\sqrt{3}}\right)^2\right]}{1 + \frac{3}{2}K\left(1 + \frac{p}{\sqrt{3}}\right)}. \tag{A7}$$

[1] J. D. Bernal, Nature (London) **183**, 141 (1959).
[2] J. D. Bernal, Nature (London) **185**, 68 (1960).
[3] J. D. Bernal, Proc. R. Soc. London, Ser. A **280**, 299 (1964).
[4] J. D. Bernal, in *Liquids: Structure, Properties, Solid Interactions*, edited by T. J. Hughel (Elsevier, Amsterdam, 1965), p. 25.
[5] J. P. Hansen and I. R. McDonald, *Theory of Simple Liquids* (Academic Press, London, 1986).
[6] M. A. Glaser and N. A. Clark, Adv. Chem. Phys. **83**, 543 (1993).
[7] M. A. Glaser, N. A. Clark, A. J. Armstrong, and P. D. Beale, *Springer Proceedings in Physics: Dynamics and Patterns in Complex Fluids* (Springer-Verlag, Berlin, 1990), Vol. 52, p. 141.
[8] J. M. Kosterlitz and D. J. Thouless, J. Phys. C **5**, L124 (1972).
[9] J. M. Kosterlitz and D. J. Thouless, J. Phys. C **6**, 1181 (1973).
[10] B. I. Halperin and D. R. Nelson, Phys. Rev. Lett. **41**, 121 (1978).
[11] D. R. Nelson and B. I. Halperin, Phys. Rev. B **19**, 2457 (1979).
[12] A. P. Young, Phys. Rev. B **19**, 1855 (1979).
[13] H. H. von Grünberg, P. Keim, K. Zahn, and G. Maret, Phys. Rev. Lett. **93**, 255703 (2004).
[14] G. Gompper and D. M. Kroll, Eur. Phys. J. E **1**, 153 (2000).
[15] R. Collins, Proc. Phys. Soc. London **83**, 553 (1964).
[16] H. Kawamura, Prog. Theor. Phys. **70**, 352 (1983).
[17] Y. M. Yi and Z. C. Guo, J. Phys.: Condens. Matter **1**, 1731 (1989).
[18] J. M. Ziman, *Models of Disorder* (Cambridge University Press, Cambridge, England, 1979).
[19] J. L. Finney, Mater. Sci. Eng. **23**, 207 (1976).
[20] G. F. Voronoi, J. Reine Angew. Math. **134**, 198 (1908).
[21] N. Metropolis, A. W. Rosenbluth, M. N. Rosenbluth, A. N. Teller, and E. Teller, J. Chem. Phys. **21**, 1087 (1953).
[22] H. Chen, D. X. Li, and K. H. Kuo, Phys. Rev. Lett. **60**, 1645 (1988).
[23] P. W. Leung, C. L. Henley, and G. V. Chester, Phys. Rev. B **39**, 446 (1989).
[24] Q. B. Yang and W. D. Wei, Phys. Rev. Lett. **58**, 1020 (1987).
[25] K. H. Kuo, Y. C. Feng, and H. Chen, Phys. Rev. Lett. **61**, 1740 (1988).
[26] S. Toxværd, Phys. Rev. Lett. **51**, 1971 (1983).
[27] S. Sengupta, P. Nielaba, and K. Binder, Phys. Rev. E **61**, 6294 (2000).
[28] K. Binder, S. Sengupta, and P. Nielaba, J. Phys.: Condens. Matter **14**, 2323 (2002).
[29] K. Zahn, A. Wille, G. Maret, S. Sengupta, and P. Nielaba, Phys. Rev. Lett. **90**, 155506 (2003).
[30] M. E. Fisher, Physics (Long Island City, N.Y.) **3**, 255 (1967).
[31] D. Stauffer, Phys. Rep. **54**, 1 (1979).
[32] D. Stauffer, *Introduction to Percolation Theory* (Taylor & Francis, London, 1985).
[33] J. Friedel, *Dislocations* (Pergamon Press, London, 1964).
[34] D. Frenkel, in *Simple Molecular Systems at Very High Density*, edited by A. Polian, P. Loubeyre, and N. Boccara (Plenum, New York, 1988).